Noninvasive Detection of Winding Short-Circuit Faults in Salient Pole Synchronous Machine With Squirrel-Cage Damper

Mauricio Cuevas, Raphael Romary, Jean-Philippe Lecointe, Fabrice Morganti, Thierry Jacq

Non-invasive Detection of Winding Short-circuit Faults in Salient-pole Synchronous Machine with squirrel-cage damper

Mauricio Cuevas[1,2], Raphaël Romary[1], Jean-Philippe Lecointe[1], Fabrice Morganti[1], Thierry Jacq[2]
[1]Univ. Artois, EA 4025, Laboratoire Systèmes Électrotechniques et Environnement (LSEE), Béthune, F-62400, France
[2]Électricité de France, EDF-Lab Paris-Saclay, Palaiseau, F-91120, France

***Abstract*—This study presents an analytical and experimental method for detecting internal turn-to-turn short circuits both in the rotor or in the stator in Salient-pole Synchronous Generator Machines (SSGM) connected to local power grid. Two main measurements are proposed to confirm or discard these electric faults: external magnetic field and External Housing Vibrations (EHV). In the event of a short-circuit winding fault, a correlation between external magnetic field and EHV is done to reinforce the diagnosis. Furthermore, the electric power injection dependency is analyzed and a non-invasive technique is proposed to determine the state of the SSGM whatever its load. Thus, it is shown that only non-invasive and on-line equipment can be used to diagnose SSGM. A diagnostic tool has been developed to show the viability of an operative wireless monitoring system on a 76MW SSGM in an industrial environment.**

***Keywords*—Diagnosis; external magnetic field; housing vibration; salient-pole synchronous machine**

I. Introduction

Hydroelectric plants, as many other power plants, are supported by environmental policies trying to reduce greenhouse effect caused by human activity. They are equipped with Salient-pole Synchronous Generator Machines (SSGM) and it is necessary to increase up-time production in order to insure electricity demand and to avoid a more polluting alternator turn-on. Establishing an adequate condition monitoring is required [1] but it generally requires invasive sensors like temperature, current sensors [2], [3], [4] or internal flux probes [5], [6], [7], [8], [9]. In synchronous machines, the stator earth fault protection does not detect turn-to-turn fault, as there is no current flowing to the ground [10]. If the generators are not initially equipped, it can be difficult to introduce invasive sensors, which do interrupt production and modify the original design of the machines [9], [11]. Only vibration sensors are currently used for non invasive monitoring of generators [12].

Monitoring techniques based on the analysis of external magnetic field have been developed in the 70s [13]. Their main advantages are the non-invasive investigation and the simplicity of implementation. However, the drawback is tied to the difficulty for modeling external magnetic field which strongly depends on the electromagnetic behavior of both the stator yoke and the motor housing, which has an important shielding effect. The external field determination requires to model the internal sources and the influence of the ferromagnetic and conducting materials of the machine. The computation of such a problem can be made using a finite element software, but an accurate modeling can be time consuming [14], [15], especially when a 3D modeling is performed. Another approach consists in adapting analytical solutions existing for simple geometries [16] but these methods, based on particular hypotheses, can be hardly exploited for electrical machines. In [17], a method based on the definition of attenuation coefficients can be easily combined with an analytical model of the machine.

Fault detection methods using the external field analysis are based on the property that any fault changes the magnetic field in the near vicinity of the machine. Difficulties for modeling and interpreting this variable leads to exploit only qualitative features of the spectrum, like the appearance of sensitive spectral lines [18]. More usually, studies on external field for fault detection are generally limited to model internal consequences of the fault such as changes in the m.m.f. distribution [19], interaction with the slotting effect [20], magnetic of electric unbalances [21]. Advanced analyses have been developed to provide a deeper information: in [22], a sophisticated inverse problem is used for fault detection, [23] shows the possibility to locate the fault whereas [24] proposes to use several flux sensors to improve the diagnosis. [11] shows that the external field can also be used to estimate the load level.

All the diagnosis methods usually require the knowledge of the healthy state of the machine regardless of the physical variable considered. The fault detection is then based on the comparison of the given state signature with the signature of the presumed healthy state by considering an indicator known to be sensitive to a fault. However, the machine load can be a disturbing factor for diagnosis because it induces several healthy states.

This paper responds to an industrial need to develop an on-line SSGM diagnosis tool in a non-invasive way, which was started in [25]. In this paper, the goal is to detect both turn-to-turn stator and rotor winding faults [26] using external magnetic flux density and external housing vibration measurements taking into account the load change effect. First, the analytical method is presented as it is improved to take in to account the SSGM with a squirrel-cage damper. The authors

also explain how the main components of both the external magnetic flux and the housing vibration are determined. The method is applied to a healthy and faultly SSGMs and the results are compared to experimental measurement obtained with a configurable SSGM. Then, the authors show that the method is applicable to any working point, that is to say for the whole ranges of active and reactive powers. It is explained how to identify the working point without using intrusive sensors. At last, the authors shows that their diagnosis strategy of non-intrusive fault detection can be embedded in a radio frequency transmitter system to diagnose a high power hydro-generator.

II. Analytical Modelling of a SSGM

The study considers a salient pole synchronous machine with dampers placed in the rotor poles as shown in Fig. 1. It also shows the simplified geometry considered for the analytical modelling. This machine has N^s and N^r slots respectively in the stator and in the rotor.

A. Healthy machine definition

The principle of this study lies the Air-gap Magnetic Flux Density (AMFD) [22], [27], named b for a so-called healthy machine, with a balanced air-gap permeance $\wp$ and a Magneto-Motive Force (MMF) ε constituted by healthy windings, given by $b(\alpha^s, t) = \wp \cdot \varepsilon$ where ε is the resulting MMF generated by the stator (ε^s) and by the rotor (ε^r). Therefore, b results from the sum of b^s and b^r: $b = b^s + b^r$. The calculation of b is based on Fourier series for $\wp$, ε^s and ε^r for a healthy SSGM and taking into account the following hypothesis :

- the stator is supplied by a three phase sine, balanced, current system,
- the rotor is supplied by a DC current,
- the effect current in the damper is neglected but the permeance due to the rotor dampers is taken into account. It will be seen that this slotting effect produces specific flux density components.

The magnitude of the flux density components depend on the stator and the rotor currents [28], but this paper is focused on the active P and reactive Q powers dependency. As b is directly linked to the stator and excitation currents and as P and Q are also linked to these currents, so b^s and b^r can be expressed in a stator referential as follows:

$$b^{s\,or\,r}(\alpha^s, t, P, Q) = \sum_{h^s\,or\,h^r} \sum_{k^s=-\infty}^{\infty} \sum_{k^r=-\infty}^{\infty} \hat{B}^{s\,or\,r}(P, Q) \cos(K^{s\,or\,r}\omega t - H^{s\,or\,r}\alpha^s) \tag{1}$$

α^s is the angular position of any point in the air-gap related to a stator reference tied to the phase 1. Considering the chosen hypotheses, the amplitudes of elementary stator and rotor flux density components $\hat{B}^s(P, Q)$ and $\hat{B}^r(P, Q)$ depend on the airgap permeance and, thus, on the toothing geometry both on stator and rotor. k^s, k^r, h^s and h^r are respectively the slotting and space harmonics resulting from Fourier series. h^s is defined by $h^s = 2\lambda + 1$ were λ is a relative integer and h^r is a positive odd integer. p and ω are the pole pair number and the rotor angular velocity ($2\pi f$, with f the frequency pulsation of the local grid). The frequency ranks K^s, K^r and the pole pair number H^s, H^r are defined by equations (2) to (5) for a healthy machine.

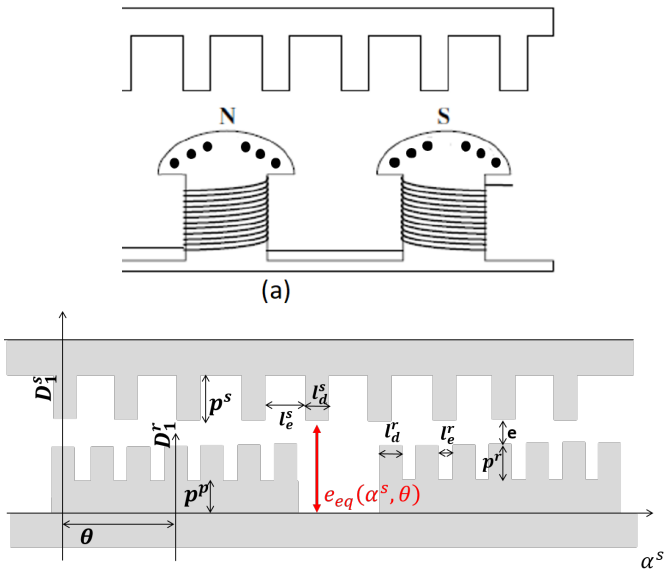

Fig. 1. (a) Real and (b) simplified geometries of the studied Synchronous Machines with two poles and six damper bars per pole.

$$K^s = 1 - (k^r N^r)/p \tag{2}$$

$$K^r = (-h^r - (k^r N^r)/p) \tag{3}$$

$$H^s = ph^s + k^s N^s + k^r N^r \tag{4}$$

$$H^r = (ph^r + k^s N^s + k^r N^r) \tag{5}$$

B. External housing vibration

Vibrations of the external housing are determined using the pressure expression (6) where μ_0 is the permeability of free space [29]. It is based on the combination of the b components.

$$F(\alpha^s, t, P, Q) = [b(\alpha^s, t, P, Q)]^2/(2\mu_0) \tag{6}$$

For a healthy SSGM, the individual mechanical deformation force $F_{K_v M}$ expressed in (7) introduces the frequency-rank K_v and and the mode number M given in (8) [30].

$$F_{K_v M} = \hat{F}_{K_v M} \cdot \cos(K_v \omega t - M\alpha^s) \tag{7}$$

$$\begin{aligned} K_v &= 2(K \pm K') \\ M &= 2(H \pm H') \end{aligned} \tag{8}$$

where K, K' and H, H' are frequency-ranks and modes of two flux density harmonics.

Fig. 2 shows both experimental and simulation model spectra of the vibration content for a 7kW, 400V, 4-poles synchronous machine, named "SM7kW4p", connected to the 50Hz local grid. Stator magnetic circuit has 36 slots filled

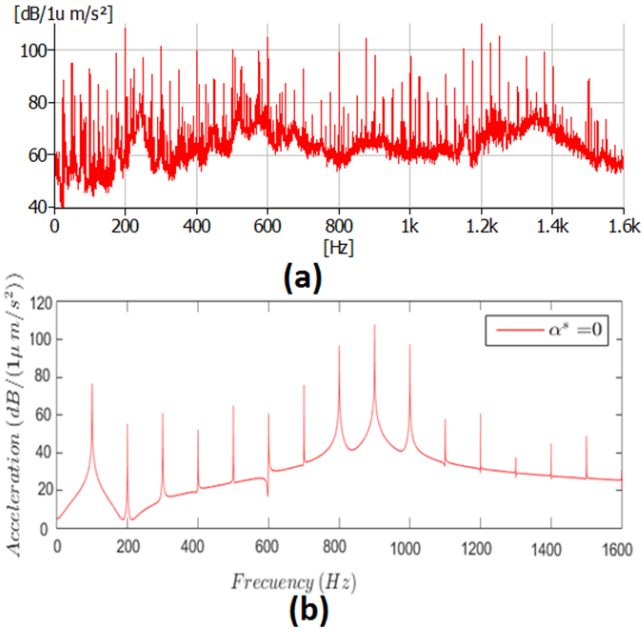

Fig. 2. (a) Experimental and (b) model spectra of the EHV content for the healthy SM7kW4p.

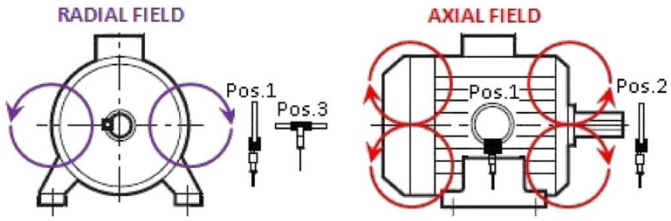

Fig. 3. Different positions (Pos.) for the search-coil around a machine. Pos.1, Pos.2 and Pos.3 capture respectively the normal, axial and tangential components of the external field

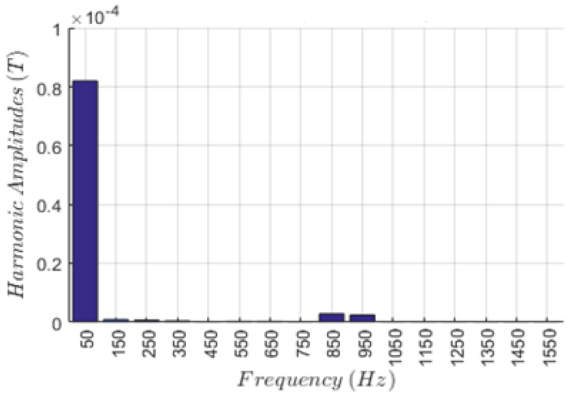

Fig. 4. Flux density components of mode 2 predicted by the analytical model.

with a distributed winding. The magnetic circuit of the rotor is salient with coils supplied by a brushless exciter. Amplitude differences of the major spectral lines between Fig. 2a and Fig. 2b are linked to mechanical structure model complexity of both the magnetic circuit and the external housing, which are composed of manifold components, for instance, bearings, various material layers and mechanical junctions. However, this simple model predicts the principal spectral-frequencies and modes in a healthy SSGM.

C. Magnetic flux density outside the SSGM

Usually, AMFD is measured indirectly by the electromotive force (EMF) induced in a search-coil. As the diagnosis is non-invasive, sensors are placed either directly against the magnetic circuit or close to the external housing. For a single flux density component $\hat{B}_{KH}$ of frequency $K\omega$, the EMF amplitude $\hat{E}_{KH}$ is proportional to $K\omega$, the turn-number N and the axial surface S of the search-coil, as shown in (9).

$$\hat{B}_{KH} = \frac{\hat{E}_{KH}}{N \cdot S \cdot K\omega} \tag{9}$$

If eddy currents and magnetic saturation effects are neglected both into magnetic circuit and into the external housing and using the magnetic wave attenuation $\nabla \times \nabla \times \mathbf{A} = \mathbf{0}$, where $\mathbf{A}$ refers to the magnetic potential introduced in Maxwell's equations, the amplitude of $\tilde{B}_{KH}$ is given by (10).

$$\tilde{B}_{KH} = \lambda_1 \cdot r^{H-1} + \lambda_2 \cdot r^{-H-1} \tag{10}$$

where r corresponds to the radial distance between the air-gap to any external point around the machine; λ_1 and λ_2 are the constants which depend both on initial conditions, on geometry of the machine and on material properties. It turns out from this last result that the higher H, the more significant the attenuation for the corresponding harmonic.

Fig. 3 shows the positions of the coil for measuring the 3 components of the flux close to the external housing. Diagnosis uses the tangential component [11] as this component gives a reliable image of the radial flux while the sensor is in front of the magnetic circuit. Fig.4 presents the EMF modes and frequencies predicted by the analytical model shows that mainly low modes dominate the spectrum, in this case only H=2 are presented in the EMF.

Fig. 5 shows simulation results of spectral e^{TAN} voltage induced in a search-coil placed on the external housing of the healthy SM7kW4p and measuring the external field tangential component. Healthy spectrum will be used as reference to determine magnetic unbalances and so to distinguish an internal winding fault. The slotting effect due to the damper is at the origin of harmonic components of frequencies 850 Hz and 950Hz.

For validating the main phenomenon described in Fig. 5, external magnetic field on the healthy SM7kW4p has been measured. The experimental test bench is shown in Fig. 6 with the SM7kW4p on a chassis and mechanically coupled to an induction machine supplied by an inverter. Results are shown in Fig. 7.

The aim of the analytical model is to identify as well as the possible external field signatures. Comparing the theoretical and experimental results of the SM7kW4p, the main harmonics are identified. The harmonics at 850Hz and 950Hz originate from the slotting effect due to the dampers. 50Hz

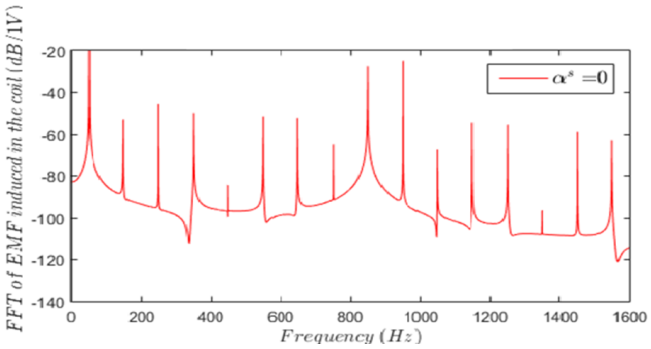

Fig. 5. Simulation model results for a healthy 7kW, 400V, 4-poles synchronous machine (SM7kW4p): e^{TAN} induced in a 1500 turns search-coil placed around the machine ($\alpha^s = 0$).

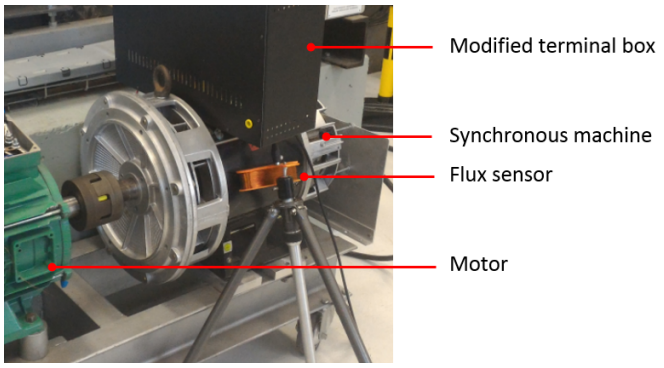

Fig. 6. Experimental test bench

and 150Hz spectrum line amplitudes are overvalued compared with experimental results. On the other hand, main differences between simulation and experimental results are harmonics of frequency multiple of 25Hz present along the spectrum. These spectrum lines are not determined with a theoretical healthy 4-poles synchronous machine given both by equations (2) and (3), because they do not consider winding asymmetries or rotor eccentricity.

III. Experimental validation in case of stator and rotor winding faults

Faults are artificially introduced in the SM7kW4p: a 12% rotor winding fault induced by a short-circuit directly switchable in the rotor and a 8% stator winding fault controlled with a resistor to limit short-circuit current to 25A. To do that, the machine has been rewound and and parts of each winding phase are accessible on a specific terminal box (Fig. 6).

A. Rotor fault AMFD contribution

Earlier studies described a rotor short-circuit fault contribution b^r_{cc} in the AMFD b_{eq} [20], [25], [28]. The fault induces a new MMF and, thus, a new air-gap flux density b^r_{cc} which generates an unbalance magnetic field in the air-gap of the SSGM, leading to b_{eq} in expression (11).

$$b_{eq}(\alpha^s, t, P, Q) = b(\alpha^s, t, P, Q) + b^r_{cc}(\alpha^s, t, P, Q) \quad (11)$$

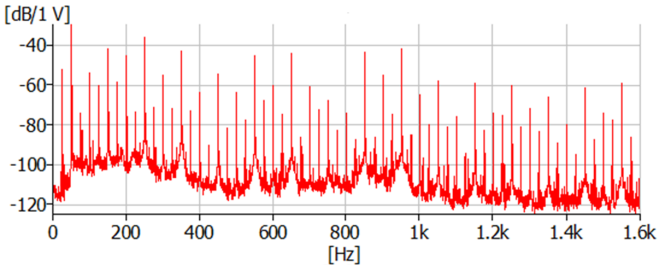

Fig. 7. SM7kW4p experimental e^{TAN} induced in a 1500 turns search-coil.

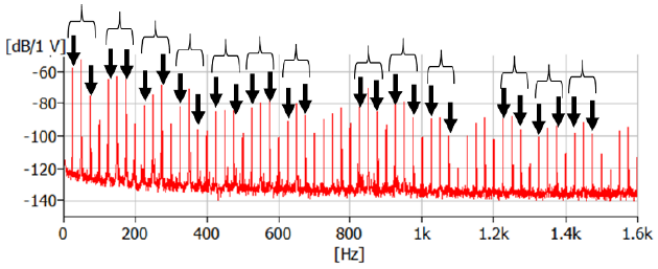

Fig. 8. e^{TAN} Experimental results on SM7kW4p with a rotor fault.

b^r_{cc} is given by (12) where $\hat{B}^r_{cc}(P,Q)$ is the Fourier series coefficient for a rotor winding fault with n^r_{cc} inter-turns short-circuited. Adopting the winding fault model given in [25], $\hat{B}^r_{cc}$ is linearly dependent of n^r_{cc} through MMF contribution ε^r_{cc}. K_{cc} and H^r_{cc} are respectively the frequency-rank (13) and the mode (14) of the considered harmonic of b^r_{cc}. New components are shown in Fig. (8).

$$b^r_{cc}(\alpha^s, P, Q, t) = \sum_{h^r=1}^{\infty}\sum_{k^s=0}^{\infty}\sum_{k^r=-\infty}^{\infty} \hat{B}^r_{cc}(P,Q)\cos\left(K^r_{cc}\omega t + H^r_{cc}\alpha^s\right) \quad (12)$$

$$K^r_{cc} = h^r/p + (k^r N^r)/p \quad (13)$$

$$H^r_{cc} = h^r + k^s N^s + k^r N^r \quad (14)$$

B. Stator fault AMFD contribution

When a turn-to-turn fault on the stator winding occurs, a new AMFD b^s_{cc} given by (15) is induced, which must be added to (1), as for (11).

$$b^s_{cc}(\alpha^s, t, P, Q) = \sum_{h^s=-\infty}^{\infty}\sum_{k^s=0}^{\infty}\sum_{k^r=-\infty}^{\infty} \hat{B}^s_{cc}(P,Q)\cos(K^s_{cc}\omega t + H_{cc}\alpha^s) \quad (15)$$

$\hat{B}^s_{cc}(P,Q)$ is the Fourier series coefficient for a turn-to-turn stator winding with n^s_{cc} inter-turns short-circuited. K^s_{cc} and H^s_{cc} in (15) are respectively the frequency-rank (16) and the pole number (17) of the considered harmonic of b^s_{cc}.

$$K^s_{cc} = 1 + (N^r k^r)/p \quad (16)$$

$$H^s_{cc} = h^s + k^s N^s + k^r N^r \quad (17)$$

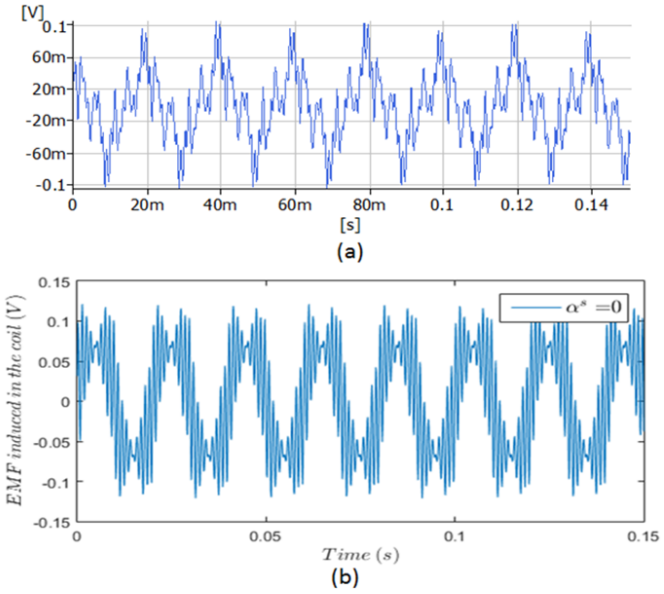

Fig. 9. SSGM with an 8% stator winding fault, a) Experimental e^{TAN} induced in an external search coil for a stator short-circuit and b) simulation model results.

In contrast to the rotor winding fault, b^s_{cc} does not introduce new frequencies to the harmonic content, but some harmonics are generated with new modes (17), especially $H = 1$, which is weakly attenuated by the stator magnetic circuit and the external housing. These harmonics will be particularly interesting for the diagnosis using external search-coils probes. Their origin can be explained by the fact that this turn-to-turn short-circuit fault doesn't rotate with respect to the stator reference. Moreover, the short-circuit current flowing in the corresponding turns creates an unidirectional magnetic field which is also found in the external magnetic field. That leads to different magnitude of the fundamental and harmonic flux density components, versus the angular position. Hence, the induced EMF in the search probe depends both on short-circuit current and on the precise place where this short-circuit into the machine occurred. Load power dependency (active and reactive power injected) will be treated in IV.

Since it hasn't been presented in previous works [25], Fig. 9 shows experimental measurements and model results of EMF induced in a search-coil for the SM7kW4p connected to the 400V local grid and with a 8% stator winding fault. It affects the fundamental component (50Hz) and creates distortions at higher frequencies, for instance, at 850Hz and 950Hz, as shown in the experimental FFT in Fig. 10a and for theoretical model in Fig. 10b. It shows that the components due to the dampers slotting is sensitive to a stator fault. Amplitude differences between experimental and simulation spectra are due to reasons explained in III-A, and because of the complexity in the estimation of the effective magnetic flux density induced in the air-gap by a stator turn-to-turn fault.

C. Rotor fault vibration contribution

Considering theoretical magnetic pressure model introduced in (6) (replacing b by b_{eq}), frequency ranks (K) and modes (M) of the forces are given by (18) and (19) for a SSGM with a rotor turn-to-turn fault. h and h' (or k and k') refer to two space (or slotting) harmonics in the Fourier series of the individual deformations of the magnetic circuit of the machine.

$$\begin{aligned} K^r_{cc1} &= -2[(h^r + h'^r) + (k^r + k'^r)]/p \\ K^r_{cc2} &= -2[(h^r - h'^r) + (k^r - k'^r)]/p \end{aligned} \tag{18}$$

$$\begin{aligned} M^r_{cc1} &= 2[(h^r + h'^r)p + (k^s + k'^s)N^s + (k^r + k'^r)N^r] \\ M^r_{cc2} &= 2[(h^r - h'^r)p + (k^s - k'^s)N^s + (k^r - k'^r)N^r] \end{aligned} \tag{19}$$

D. Stator fault vibration contribution

Carrying out a similar procedure done for a rotor fault, it is interesting to discriminate each individual harmonic content of global deformations in the case of a stator winding fault. Indeed, (20) and (21) show that, likewise in the study of magnetic flux density, a stator short-circuit fault modifies the existing frequency-ranks and modes which are in the vibration content of a healthy SSGM. Expression (7) can still be used, which leads to:

$$\begin{aligned} K^s_{cc1} &= 2[1 + (k^r + k'^r)] \\ K^s_{cc2} &= 2[k^r - k'^r] \end{aligned} \tag{20}$$

$$\begin{aligned} M^s_{cc1} &= 2[(h^s + h'^s)p + (k^s + k'^s)N^s + (k^r + k'^r)N^r] \\ M^s_{cc2} &= 2[(h^s - h'^s)p + (k^s - k'^s)N^s + (k^r - k'^r)N^r] \end{aligned} \tag{21}$$

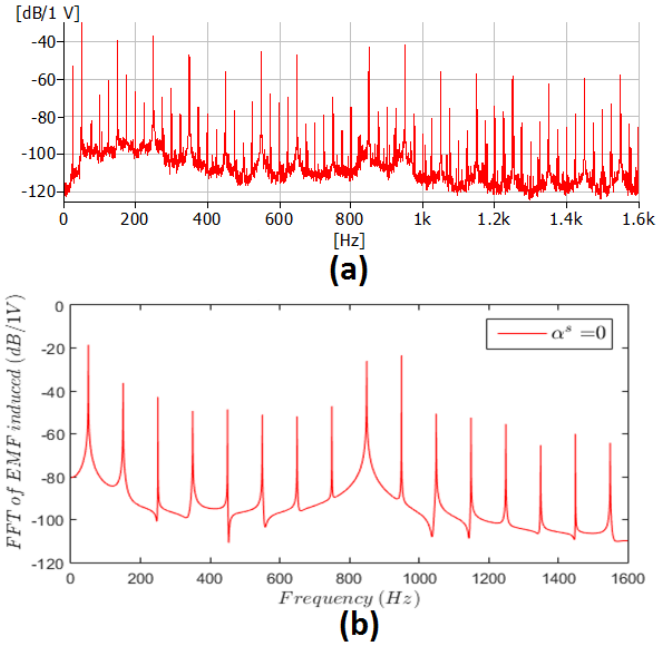

Fig. 10. (a) Experimental and (b) simulation model spectra of e^{TAN} for the SM7kW4p with an 8% stator winding fault.

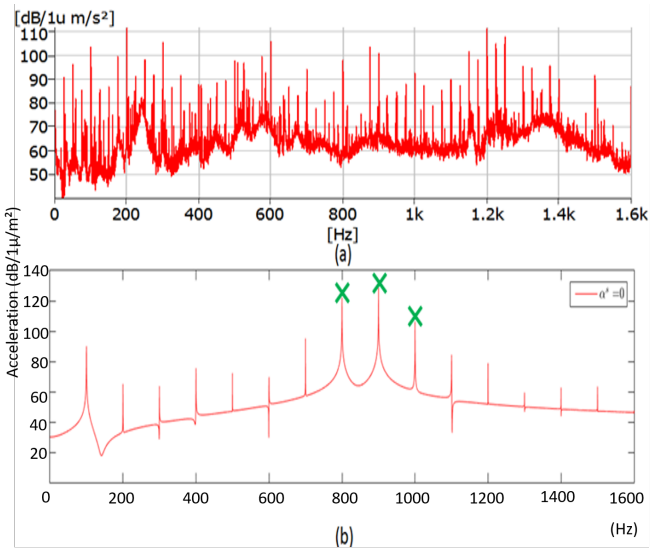

Fig. 11. (a) Experimental and (b) simulation model spectra of EHV for the SM7kW4p connected to 400V local grid with an 8% stator winding fault.

Fig. 11 gives the Fourier transform of the experimental results (a) and the model results (b) of the EHV for a SSGM connected to the 400V local grid. In this case, the machine operates $P = 3\text{kW}$ and $Q = 1,5\text{kVAR}$. Even if all amplitudes of the spectra of the simulation model do not match with the experimental results, this figure enables to validate the theoretical model which takes into account the main frequencies and modes.

IV. Tests on load

The diagnosis procedure is based on comparisons between the spectra measured continuously and the healthy spectrum, which must be previously measured for the same SSGM and without displacing the sensors. Therefore, as SSGM regime (electric power) changes, the magnetic content might varies as well, impacting the EHV and external field.

The first step is to analyze the impact and the influence on both the external field and the EHV for a SSGM face to different injected or absorbed electric power. To do that, the SM7kW4p is coupled with a motor drive which transmits mechanical power through the shaft and active power is injected to the grid. Active P and reactive Q powers are controlled by the torque of the motor drive and the DC rotor excitation.

Analysis is focused on the study of the harmonic content in order to visualize the impact, varying P and Q, on some sensitive spectral lines of each magnitude measured given by (18) and (20), and thus to recognize a fault by comparing the spectra of healthy and faulty states. As previously, the two types of inter-turn short-circuit are considered, 12% rotor winding fault and 8% stator winding fault.

Then, the second goal is to show how it is possible to identify the operating point of the machine, always using non-intrusive sensors.

A. Rotor winding fault in a SSGM

Fig. 12 shows how EMF and EHV are modified compared to the healthy state for two frequencies chosen as examples from equation (13). Likewise, other frequencies could be shown, but these two frequencies, predicted with the analytical modeling (15) represent the overall behavior of the spectrum lines introduced by this rotor fault. These two theoretical sensitive frequencies do not exist in the spectrum for the healthy SM7kW4p but there are not absolutely equal to zero as shown in Fig. 12a and Fig. 12b with the grey scale surfaces established with P and Q. The orange surfaces concern all states for a 12% rotor turn-to-turn winding fault. For an alike Q, EMF remains almost constant along P. Indeed, as shown in Fig. 12a, maximum differences between healthy and faulty states reach 15 times for $Q = 2\text{kVAR}$. Hence, the greater the reactive power injected, the larger the gap between both states. In other words, when the machine is injecting reactive power, the rotor fault is flagrant and, thus, easier to detect. Even though, at high consumed reactive power ($Q \ll 0$), this specific frequency is still sensible in order to detect the

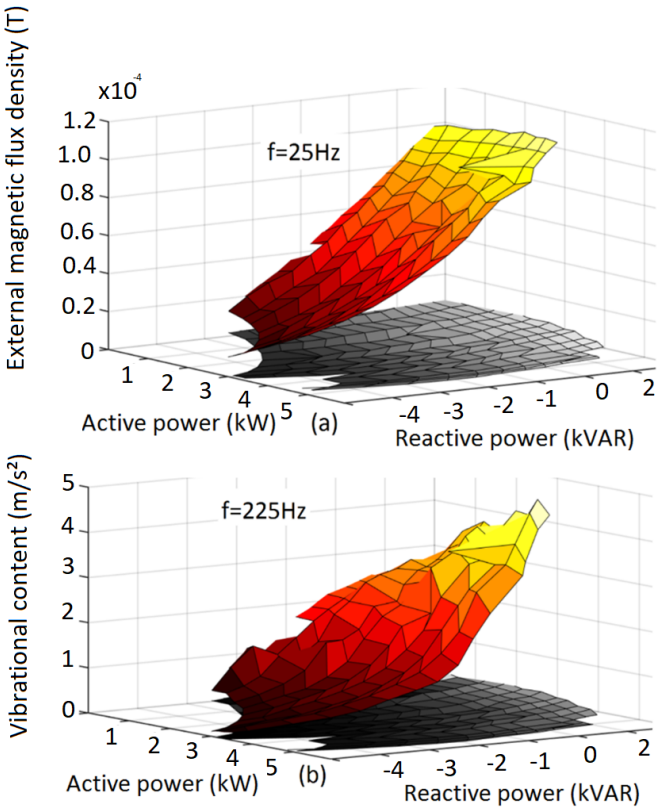

Fig. 12. Load tests for the SM7kW4p with a 12% rotor winding fault. Healthy state in grey and rotor faulty state in orange for (a) External flux density and (b) EHV

.

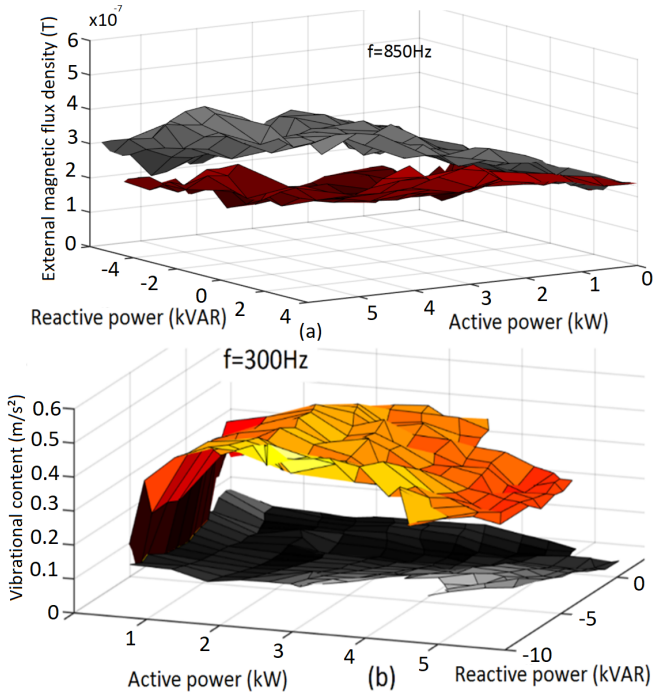

Fig. 13. Load tests for the SM7kW4p with an 8% stator winding fault machine. Healthy states in grey and stator faulty state in orange for (a) External flux density and (b) EHV .

rotor fault. At $Q = -9\text{kVAR}$ and any active power, EMF differences are around 1.3 times, which is still measurable.

EHV differences between the two states have the same tendency than EMF, which is logic because of the strong link between EHV and EMF. In Fig. 12b, 225Hz spectral components show a positive trend according to reactive power increase. Extreme different values begin at 2 times for $Q = 9\text{kVAR}$ and arise about 25 times for $Q = 2\text{kVAR}$.

As a result, the load variations do not influence the rotor fault detection for any P and Q, as the analyze is done on components with high amplitude modifications.

B. Stator winding fault in a SSGM

Fig. 13 shows two sensitive frequencies (from equation (15)) for the SM7kW4p with a 8% stator winding fault. Analogously to IV-A, these sensitives frequencies frequencies show reliably the main behavior of all sensitive frequencies predicted by the theoretical description of the stator fault. In contrast with IV-A, they are theoretically present in the EMF spectrum for the healthy SM7kW4p. Moreover, it can be observed from Fig. (13) that the fault tends to reduce the sensitive component. Thus, compared with the rotor fault, a higher accuracy is required to detect differences between healthy and faulty spectra. In this case, variations of both EMF and EHV are more subordinated to the active power than to reactive power.

In Fig.13a for a healthy machine (grey line), 850Hz EMF component varies from 0.1µT to 0.05µT along the active power for any reactive power. For a given active power, external flux density remains almost constant, i.e. maximum variation along Q for an alike P is less than 8µT. Mean difference between healthy and faulty states is approximately constant for any P and Q, around 0.075µT gap. For the vibration content, Fig. 13b shows the 300Hz EHV differences between healthy and faulty states with P and Q. The ratio is about 33 times, which is measurable within the sensibility of current accelerometers.

C. Electric power dependency

As it has been shown that the faults can be determined by comparing spectra at a given operating point, the next difficulty is to identify the working points on all the P and Q ranges in a non intrusive way. Indeed, the external magnetic signature measured by a sensor varies with P and Q. That is why the magnetic signature can translate a load change or a fault which appears. Thus, to separate the two possibilities, it is necessary to identify the working point of the machine. The aim is to associate to the healthy state, one signature for each working point. The principle which is applied here doesn't consist in searching the exact values of P and Q. EMF coils placed in tangential and axial positions are used to obtain an image e^{TAN} of AMFD, as it is done for the diagnosis, and an image e^{AX} (Pos. 2 in Fig. 2) of the field due to the currents in both stator and inductor. Here, only the 50Hz fundamental components $e^{TAN}_{(1)}$ and $e^{AX}_{(1)}$ are analyzed. Amplitudes $E^{AX}_{(1)}$ and $E^{TAN}_{(1)}$, as well as $\Phi_{E^{TAN}_{(1)},E^{AX}_{(1)}}$ which is the phase-shift angle between $e^{AX}_{(1)}$ and $e^{TAN}_{(1)}$ are shown in Figs. 14, 15 and 16 with P and Q variations.

As it can be seen that, for each (P,Q) pair, an unique triplet $\left(E^{AX}_{(1)}, E^{TAN}_{(1)}, \Phi_{e^{TAN}_{(1)},e^{AX}_{(1)}}\right)$ appears, highlighting a bijection between the load and these measurements. Thus, each measurement using external search coils corresponds to an unique loading point, which allows to distinguish all operational points.

V. Non-invasive diagnostic system applied to a 76MW hydro-generator

A. External magnetic content of a 76 MW hydro-generator

The diagnosis method has been applied to a 76MW, 600rpm, 10 poles SSGM, named "SM76MW10p" (Table I) and installed in a hydro-power plant. Currently, the machine operates as alternator injecting power to the local grid but no-faults can be produced as in the case of SM7kW4p. Only reactive power control is set by DC rotor current. As there is no control of the hydro-turbine, active power is always maximum.

The SM76MW10p has been equipped, during a maintenance period, of sensors made of two search-coils to measure simultaneously the tangential and axial components of the flux. They are placed in the middle of the housing, the first which measures $e^{AX,ext}$ and $e^{TAN,ext}$ is outside the machine against the housing while the second which measures $e^{AX,int}$ and $e^{TAN,int}$ is between the housing and the magnetic circuit. Fig. 17 shows the top of the machine placed in vertical position and

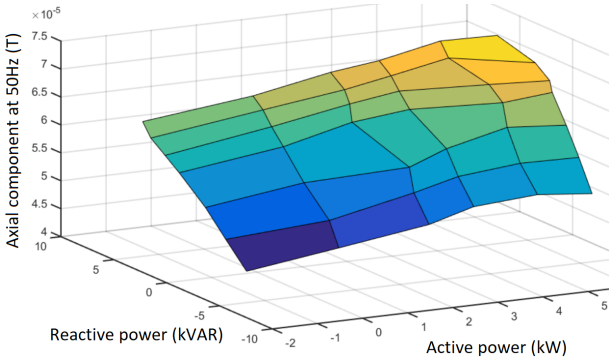

Fig. 14. Variations of $E^{AX}_{(1)}$ with P and Q.

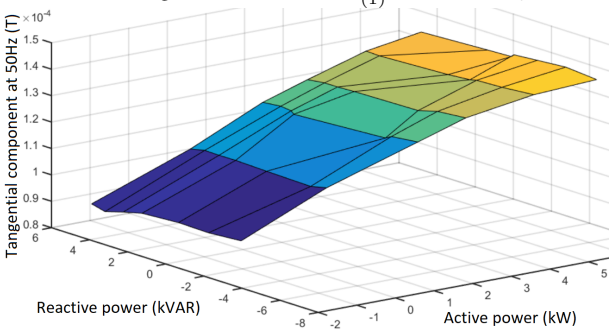

Fig. 15. Variations of $E^{TAN}_{(1)}$ with P and Q.

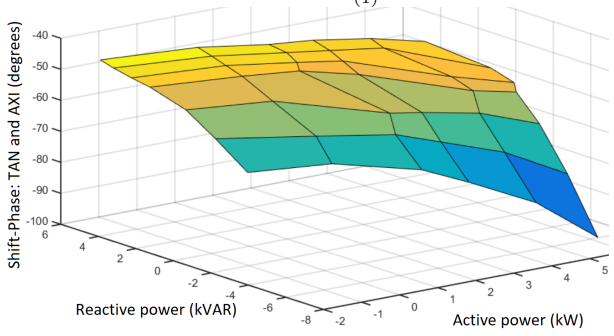

Fig. 16. Variations of $\Phi_{e^{TAN}_{(1)},e^{AX}_{(1)}}$ with P and Q.

a sensor wound around a printed media stuck on the machine with magnets. Fig. 18 shows that $e^{TAN,int}$, in addition to principal harmonics (150, 250, 350Hz, etc) has harmonics which are multiple of 10Hz along the spectrum although they theoretically do not exist in a healthy machine. As the machine has 10 salient poles, they may be explained by a possible short-circuit, using equation (13) for $h^r = 1$ and $k^r = 0$ with $p = 5$). For instance, both 40Hz and 60Hz spectrum-line amplitudes have to be monitored in particular due to their high value compared to others sensible spectrum-lines multiple of 10.

TABLE I
MAIN FEATURES OF 76MVA.

Complex power	85MVA
Reactive power	38, 06MVAR
Phase-phase voltage	26, 85kV
Stator Current	3166A
Frequency	50Hz
Rate speed	300rpm
Pole number	10
External diameter	3, 97m

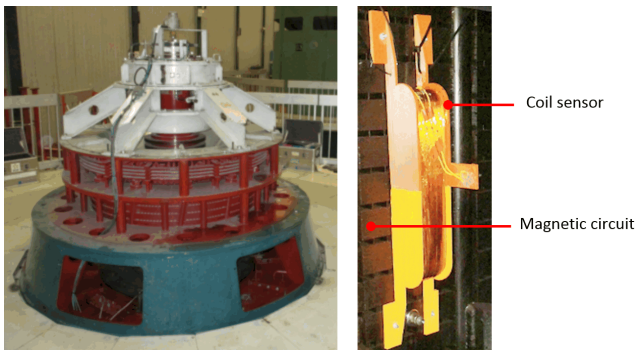

Fig. 17. Top view of the 76MW hydro-generator and sensor installed against the magnetic circuit

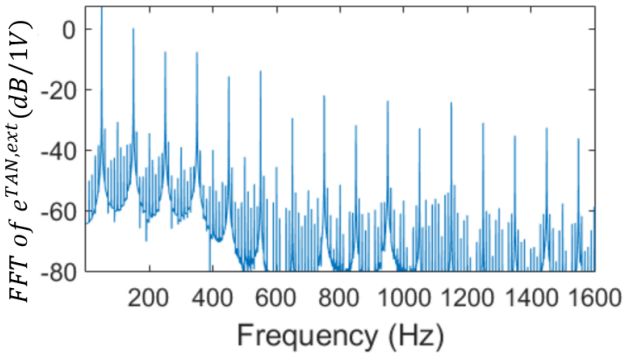

Fig. 18. Experimental $e^{TAN,int}$ in a 1000 turns search-coil for the SM76MW10p.

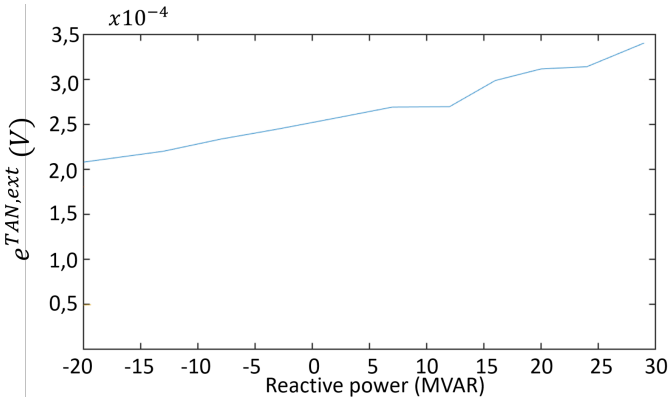

Fig. 19. Variations of $e^{TAN,ext}_{(1)}$ with Q for the SM76MW10p.

Then, Fig. 19 shows how the external $b^{TAN,ext}_{(1)}$ fundamental tangential component of the flux density increases practically linear along Q analogously to SM7kW4p. Fig. 20 shows $\Phi_{e^{TAN,ext}_{(1)},e^{AX,ext}_{(1)}}$ between $e^{TAN,ext}_{(1)}$ and $e^{AX,ext}_{(1)}$) with Q. The external signals are easier to analyze compared to the signals from sensors between the magnetic circuit and the

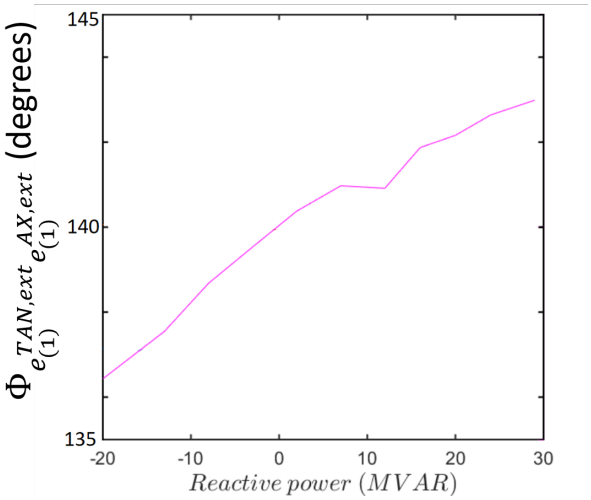

Fig. 20. Variations of $\Phi_{\Phi_{(1)}^{TAN,ext},e_{(1)}^{AX,ext}}$ with Q.

housing. The reason is that $E_{(1)}^{AX,ext}$ is very low at this place as the flux is mainly radial. It can be seen that $\Phi_{e_{(1)}^{TAN,ext},e_{(1)}^{AX,ext}}$ increases, as measured for the SM7kW4p. It is in accordance with the variation with Q of the phase shift angle between the stator single phase voltage and the current. The values of $\Phi_{e_{(1)}^{TAN,ext},e_{(1)}^{AX,ext}}$ are different from expected ones, similar to angle between stator voltage and current, for two reasons:

- First, the axial search-coil gives an image of the phase current but because of the derivative effect of the search coil, as a results, 90° have to be added to the phase of $e_{(1)}^{AX,ext}$ and thus to $\Phi_{e_{(1)}^{TAN,ext},e_{(1)}^{AX,ext}}$. Rather, $e_{(1)}^{TAN,ext}$ has not to be corrected since the tangential component is an image of phase-voltage.
- Second, the field which crosses the massive parts of the housing is phase-shifted. As the housing is not the same all around the machine, the phase shifting is different for the axial and tangential components. However, the effect is constant with the frequency, which doesn't affect the measurement of $\Phi_{e_{(1)}^{TAN,ext},e_{(1)}^{AX,ext}}$.

These measurements confirm that the external field is fully exploitable to identify, even with a high power synchronous generator, the working conditions.

B. System for non-invasive diagnosis

Fig. 21 shows an on-line and non-invasive prototype diagnosis system able to monitor SSGM. This prototype exploits external magnetic field and housing vibration, with the purpose of detecting internal magnetic unbalances in the machine due to winding faults. Spectral correlation of these magnitudes are performed in a microcomputer in order to confirm or discard an eventual internal winding short-circuit either in the rotor or in the stator. The system analyzes the differences between the reference and measured states for some sensitive frequencies of EMF and EHV, and for each load power injection point

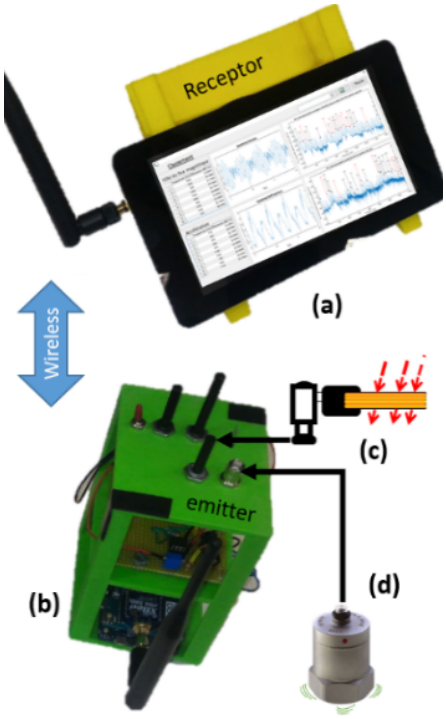

Fig. 21. Wireless diagnostic system. (a) Microcomputer (b) EMFD and EHV (c) Search coil (d) Accelerometer.

(P and Q). A portable screen shows the most affected spectral lines by a possible short-circuit fault. According to the correlation established in IV, a diagnosis software computes a failure probability so that a rapid diagnosis condition is given wireless ([31]) to the power plant operator of the machine. This technical solution includes two main components:

- An arduino DUE programmed to receive and to digitize, using a AD converter (8bits at 19,2kb/s), the EMF and acceleration signals. Then, it transmits these signals by wireless transmission.
- A Raspberry Pi responsible on receiving the signals from the Arduino DUE. It computes the FFT, correlates these spectra in order to identify magnetic imbalances in the generator using a program coded in Python.

VI. Conclusion

A diagnostic based on two non-invasive measurements has been presented. It allows to identify either a rotor or stator turn-to-turn winding fault, even if operating point varies. The correlation between the external field and the EHV makes it possible to increase the reliability of the global method in order to confirm or discard an eventual internal magnetic unbalance. Loading tests have been accomplished to evaluate the influence of active and reactive powers on the fault detection. The non-intrusive characteristic of the method is continued with the identification of the SSGM load by comparing external flux components. Finally, an on-line and non-invasive electronic tool has been implemented in order to diagnose SSGM in industrial environment so that a first and rapid health status

condition can be given to power producers. The proposed method can be applied to detect other kinds of faults as turn to ground fault or eccentricity as they appear in the external magnetic field. In case of a turn to ground fault, the stator ground fault protection will act immediately but the fault protection are unable to detect turn to turn faults. The probes used in this paper to detect the stator and rotor turn-to-turn faults can be used to detect them. The further work will consist in identifying the reference spectra and in separating the different kinds of faults.

ACKNOWLEDGMENT

This work is supported by MEDEE program supervised by the French national technological research cluster on electrical machine efficiency increase. This program including Electricité de France (EDF) is sponsored by Hauts-de-France region (France) and the European founds (FEDER).

REFERENCES

[1] H. A. Toliyat and G. B. Kliman, *Handbook of electric motors*. CRC press, 2004, vol. 120.

[2] O. Kokoko, A. Merkhouf, A. Tounzi, K. Al-Haddad, and E. Guillot, "Analysis of air-gap influence on a large hydro generator's parameters using sudden symmetrical short-circuit test," in *2015 IEEE International Electric Machines Drives Conference (IEMDC)*, May 2015, pp. 102–107.

[3] S. Nandi, H. A. Toliyat, and X. Li, "Condition monitoring and fault diagnosis of electrical motors-a review," *IEEE Transactions on Energy Conversion*, vol. 20, no. 4, pp. 719–729, Dec 2005.

[4] A. Sapena-Ba, M. Pineda-Sanchez, R. Puche-Panadero, J. Martinez-Roman, and D. Mati, "Fault diagnosis of rotating electrical machines in transient regime using a single stator current," *IEEE Transactions on Instrumentation and Measurement*, vol. 64, no. 11, pp. 3137–3146, Nov 2015.

[5] T. Ghanbari and A. Farjah, "A magnetic leakage flux-based approach for fault diagnosis in electrical machines," *IEEE Sensors Journal*, vol. 14, no. 9, pp. 2981–2988, Sept 2014.

[6] K. T. Kim, S. T. Lee, and J. Hur, "Diagnosis technique using a detection coil in bldc motors with interturn faults," *IEEE Transactions on Magnetics*, vol. 50, no. 2, pp. 885–888, Feb 2014.

[7] M. Biet, "Rotor faults diagnosis using feature selection and nearest neighbors rule: Application to a turbogenerator," *IEEE Transactions on Industrial Electronics*, vol. 60, no. 9, pp. 4063–4073, Sept 2013.

[8] A. Bacchus, A. Tounzi, J. P. Argaud, B. Bouriquet, M. Biet, L. Macaire, and Y. L. Menach, "Estimation of fem model parameters using data assimilation and its application to an electrical machine," *IEEE Transactions on Magnetics*, vol. 52, no. 3, pp. 1–4, March 2016.

[9] R. E. Caetano, I. E. Chabu, G. Stolfi, J. C. Santos, S. Nagao, C. E. Gomes, R. D. Paiva, S. I. Nabeta, and F. J. Micerino, "Development of distance sensors for diagnosing air-gap anomalies in synchronous generators," in *2015 IEEE 24th International Symposium on Industrial Electronics (ISIE)*, 2015, pp. 146–149.

[10] K. A. Jaafari, A. Negahdari, H. A. Toliyat, N. Safari-Shad, and R. Franklin, "Modeling and experimental verification of a 100% stator ground fault protection based on adaptive third-harmonic differential voltage scheme for synchronous generators," *IEEE Transactions on Industry Applications*, vol. 53, no. 4, pp. 3379–3386, July 2017.

[11] F. Zidat, J.-P. Lecointe, F. Morganti, J.-F. Brudny, T. Jacq, and F. Streiff, "Non invasive sensors for monitoring the efficiency of ac electrical rotating machines," *Sensors*, vol. 10, no. 8, pp. 7874–7895, 2010.

[12] W. Q. Lim, D. H. Zhang, J. H. Zhou, P. H. Belgi, and H. L. Chan, "Vibration-based fault diagnostic platform for rotary machines," in *IECON 2010 - 36th Annual Conference on IEEE Industrial Electronics Society*, Nov 2010, pp. 1404–1409.

[13] D. Thompson, J. Greig, P. J. Tavner, P. Hammond, and J. Penman, "Contribution to the study of leakage fields at the ends of rotating electrical machines," *Electrical Engineers, Proceedings of the Institution of*, vol. 126, no. 9, pp. 840–, September 1979.

[14] A. Kameari, "Three-dimensional eddy current calculation using finite element method with a-v in conductor and omega; in vacuum," *IEEE Transactions on Magnetics*, vol. 24, no. 1, pp. 118–121, Jan 1988.

[15] N. P. Kumar, T. Isha, and P. Balakrishnan, "Radial electro-magnetic field analysis of induction motor under faulty condition using fem," in *2016 Biennial International Conference on Power and Energy Systems: Towards Sustainable Energy (PESTSE)*, Jan 2016, pp. 1–6.

[16] A. Canova, A. Manzin, and M. Tartaglia, "Evaluation of different analytical and semi-analytical methods for the design of elf magnetic field shields," *IEEE Transactions on Industry Applications*, vol. 38, no. 3, pp. 788–796, May 2002.

[17] Romary, R., Roger, D., and Brudny, J.-F., "Analytical computation of an ac machine external magnetic field," *Eur. Phys. J. Appl. Phys.*, vol. 47, no. 3, p. 31102, 2009.

[18] L. Frosini, S. Zanazzo, A. Albini, and M. Ferraris, "An experimental investigation of the high frequency effects in low voltage electrical drives," in *2017 IEEE 11th International Symposium on Diagnostics for Electrical Machines, Power Electronics and Drives (SDEMPED)*, Aug 2017, pp. 97–103.

[19] H. Henao, C. Demian, and G.-A. Capolino, "A frequency-domain detection of stator winding faults in induction machines using an external flux sensor," *IEEE Transactions on Industry Applications*, vol. 39, no. 5, pp. 1272–1279, 2003.

[20] R. Romary, R. Corton, D. Thailly, and J. Brudny, "Induction machine fault diagnosis using an external radial flux sensor," *The European Physical Journal Applied Physics*, vol. 32, no. 2, pp. 125–132, 2005.

[21] O. Vitek, M. Janda, V. Hajek, and P. Bauer, "Detection of eccentricity and bearings fault using stray flux monitoring," in *8th IEEE Symposium on Diagnostics for Electrical Machines, Power Electronics Drives*, Sept 2011, pp. 456–461.

[22] L. Schmerber, L.-L. Rouve, and A. Foggia, "Original 2d cylindrical harmonics method for identification of the near magnetic stray field of electrical motor," in *Electric Machines and Drives, 2005 IEEE International Conference on*. IEEE, 2005, pp. 92–98.

[23] J. Penman, H. G. Sedding, B. A. Lloyd, and W. T. Fink, "Detection and location of interturn short circuits in the stator windings of operating motors," *IEEE Transactions on Energy Conversion*, vol. 9, no. 4, pp. 652–658, Dec 1994.

[24] M. Irhoumah, R. Pusca, E. Lefevre, D. Mercier, R. Romary, and C. Demian, "Information fusion with belief functions for detection of interturn short-circuit faults in electrical machines using external flux sensors," *IEEE Transactions on Industrial Electronics*, vol. 65, no. 3, pp. 2642–2652, March 2018.

[25] M. Cuevas, R. Romary, J.-P. Lecointe, and T. Jacq, "Non-invasive detection of rotor short-circuit fault in synchronous machines by analysis of stray magnetic field and frame vibrations," *IEEE Transactions on Magnetics*, vol. 52, no. 7, pp. 1–4, 2016.

[26] A. Berzoy, A. Mohamed, and O. Mohammed, "Complex-vector model of inter-turn failure in induction machines for fault detection and identification," *IEEE Transactions on Industry Applications*, 2016.

[27] L. Frosini, A. Borin, L. Girometta, and G. Venchi, "Development of a leakage flux measurement system for condition monitoring of electrical drives," in *Diagnostics for Electric Machines, Power Electronics & Drives (SDEMPED), 2011 IEEE International Symposium on*. IEEE, 2011, pp. 356–363.

[28] M. Cuevas, R. Romary, J. P. Lecointe, F. Morganti, and T. Jacq, "Non-invasive detection of winding short-circuit faults in salient-pole synchronous machine," in *2017 IEEE International Electric Machines and Drives Conference (IEMDC)*, May 2017, pp. 1–7.

[29] J. Le Besnerais, "Vibroacoustic analysis of radial and tangential air-gap magnetic forces in permanent magnet synchronous machines," *IEEE Transactions on Magnetics*, vol. 51, no. 6, pp. 1–9, 2015.

[30] B. Cassoret, J.-P. Lecointe, and J.-F. Brudny, "Influence of the pole number on the magnetic noise of electrical ac machines," *Progress In Electromagnetics Research B*, vol. 33, pp. 83–97, 2011.

[31] F. Morganti, M. O. Younsi, M. Cuevas, J. P. Lecointe, and T. Jacq, "Using arduino development platform in the diagnosis of ac electrical machines," in *2017 IEEE International Conference on Environment and Electrical Engineering and 2017 IEEE Industrial and Commercial Power Systems Europe (EEEIC / I CPS Europe)*, June 2017, pp. 1–6.

Mauricio Cuevas was born in 1985. He received his electrical engineering diploma in the University of Chile (2010), and he obtained two Master degrees in France: in electrical engineering and in nuclear fusion technology. He received his Ph.D. from the Artois University concerning fault diagnosis in large electric alternators in 2017. He has currently a Post-doc position in Max-Planck-Institut for Plasma Physics (Germany) working on the electrical arrangement of a new high couple divertor coil with the fusion plasma current.

Raphaël Romary (M'10) received the Ph.D. from Lille University, Lille, France, in 1995 and the D. SC degree from Artois University, Bthune, France, in 2007. He is currently a Full Professor in Artois University and a Researcher at the Laboratory of Electrical Systems and Environment (LSEE). His research interest concerns the analytical modeling of electrical machines with applications to noise and vibration, losses, electromagnetic emissions, diagnosis.

Jean-Philippe Lecointe (M04) received the MSc degree in Electrical Engineering from Lille University in 2000. He received the PhD degree and the DSc degree from the Artois University, France, in 2003 and 2012. He is currently Full Professor in Electrical Engineering at Artois University. He is the head of the Environnement and Electrical Systems research Lab.

Fabrice Morganti received his PhD degree in 1994 from The Lille-I University, France. He is Associate Professor at the Artois University at the LSEE (Electrical Systems and Environment Research Laboratory), France. His research interests focus on monitoring AC machines by using non-invasive methods in wide band frequency with low-cost embedded systems.

Thierry Jacq obtained his Engineer degree at the Institut National Polytechnique de Grenoble, France. In 1998, he joined the Research and Development division of EDF. His research interests include condition monitoring and diagnostic tools of electrical machines.